

## A methodology for assessing fatigue life of a countersunk riveted lap joint

Gang Li<sup>\*1</sup>, Guillaume Renaud<sup>1a</sup>, Min Liao<sup>1b</sup>, Takao Okada<sup>2c</sup> and Shigeru Machida<sup>2d</sup>

<sup>1</sup>*Aerospace, National Research Council, Canada*

<sup>2</sup>*Aeronautical Technology Directorate, Japan Aerospace Exploration Agency, Japan*

*(Received November 7, 2015, Revised January 6, 2016, Accepted January 7, 2016)*

**Abstract.** Fatigue life prediction of a multi-row countersunk riveted lap joint was performed numerically. The stress and strain conditions in a highly stressed substructure of the joint were analysed using a global/local finite element (FE) model coupling approach. After validation of the FE models using experimental strain measurements, the stress/strain condition in the local three-dimensional (3D) FE model was simulated under a fatigue loading condition. This local model involved multiple load cases with nonlinearity in material properties, geometric deformation, and contact boundary conditions. The resulting stresses and strains were used in the Smith-Watson-Topper (SWT) strain life equation to assess the fatigue “initiation life”, defined as the life to a 0.5 mm deep crack. Effects of the rivet-hole clearance and rivet head deformation on the predicted fatigue life were identified, and good agreement in the fatigue life was obtained between the experimental and the numerical results. Further crack growth from a 0.5 mm crack to the first linkup of two adjacent cracks was evaluated using the NRC in-house tool, CanGROW. Good correlation in the fatigue life was also obtained between the experimental result and the crack growth analysis. The study shows that the selected methodology is promising for assessing the fatigue life for the lap joint, which is expected to improve research efficiency by reducing test quantity and cost.

**Keywords:** fatigue life; global/local FE model coupling; crack growth; riveted lap joint; the Smith-Watson-Topper (SWT) equation

### 1. Introduction

The damage tolerance philosophy is widely applied to aerospace structures for safe aircraft operation through maintenance programs. Engineering data in crack nucleation and growth behaviours during operation is the base to assess the structural fatigue life (Skorupa and Skorupa 2012), the cracks found at multiple sites show widespread fatigue damage (WFD) behaviour. The number of cycles from the first operation day to a dominant crack with certain length, defined as the “initiation” life, can be used in the WFD evaluation. Better understanding in WFD directly

---

\*Corresponding author, Ph.D., E-mail: [Gang.Li@nrc-cnrc.gc.ca](mailto:Gang.Li@nrc-cnrc.gc.ca)

<sup>a</sup>Ph.D., E-mail: [Guillaume.Renaud@nrc-cnrc.gc.ca](mailto:Guillaume.Renaud@nrc-cnrc.gc.ca),

<sup>b</sup>Ph.D., E-mail: [Min.Liao@nrc-cnrc.gc.ca](mailto:Min.Liao@nrc-cnrc.gc.ca)

<sup>c</sup>E-mail: [okada.takao@jaxa.jp](mailto:okada.takao@jaxa.jp),

<sup>d</sup>E-mail: [machida.shigeru@jaxa.jp](mailto:machida.shigeru@jaxa.jp)

contributes to improvement of the application of the damage tolerance philosophy (Grandt, Farris Jr. *et al.* 1999, Eastaugh, Straznicky *et al.* 2000, Silva *et al.* 2000, Trego and Cope 2001, Anderson *et al.* 2004), WFD evaluation is often limited to specific cases and its method is not widely established yet. The existing literature (Liao, Shi *et al.* 2001, Liao, Bombardier *et al.* 2010, Bombardier, Liao *et al.* 2010, Huang, Wang *et al.* 2012, Newman Jr. and Ramakrishnan 2015) shows that there is a limited number of quantitative studies available in joint fatigue life assessment using the stress and strain induced by the combination of joint manufacturing process and external cyclic loading. To fill this knowledge gap and improve the accuracy of the joint fatigue life prediction, the National Research Council Canada (NRCC) and Japan Aerospace Exploration Agency (JAXA) jointly conducted research work for the fatigue life prediction, followed a WFD evaluation through testing of a triple-row countersunk riveted fuselage lap joint.

This paper presents the assessment of the fatigue “initiation” life (to an approximately 0.5 mm crack) for the JAXA riveted flat panel test structure, considering the combined effects of joint manufacturing and external cyclic loading conditions. Joint manufacturing factors such as the rivet-hole clearance and rivet driven head deformation were considered, since they directly affect the joint integrity condition (Müller 2000, Szolwinski and Farris 2000), The stresses and strains induced by the manufacturing and external cyclic loading conditions were obtained using contact finite element (FE) models (Li and Shi 2004, Li, Shi *et al.* 2007, 2011, 2012) through a global/local FE model coupling approach (MSC/Patran),

This work was conducted using the Smith-Watson-Topper (SWT) strain-life method (Smith, Watson *et al.* 1970), Displacement fields obtained from the global FE model were used as the remote loading applied to a local 3D FE model after the simulation of the riveting process. Each simulation consisted of multiple loading steps, including rivet squeezing and releasing, and then remote cyclic loading. A cyclic stress-strain curve was used in the local model (Boller and Seeger 1987), Stresses and strains extracted from the local FE model at the third cycle were then used to calculate the joint fatigue crack initiation life via the SWT equation. The effects of the rivet head deformation and rivet-hole clearance on calculated fatigue life were studied. The NRC in-house tool, CanGROW, was then used to carry out a preliminary Monte Carlo simulation for the fatigue life distribution to the first link-up between cracks. It involved the development of correction factors to include the countersunk geometry and the post-riveting residual stresses effects in the simulations.

## 2. Experimental information

Information about the experimental lap joint geometry, configuration, and strain gauge (SG) locations is shown in Fig. 1. Only one joint was tested for fatigue life evaluation. Based on a JAXA panel joint drawing provided to NRC, the rivet hole diameter was  $4.039 \pm 0.127$  mm (max: 4.166 mm, min: 3.912 mm, note the minimum size could cause an interference fit), The riveted lap joint consisted of two 1.27 mm thick Al 2024-T3 alloy panel sheets and one 1.6 mm thick and 20 mm wide Al 2024-T3 alloy strap attached to the middle row to simulate a fuselage panel stringer. This joint was riveted by 3 rows of 20 fasteners, including 9 button head rivets installed on both sides of the panel and MS20426AD5-5 42 countersunk rivets in the remaining central locations, where the joint multiple-site damages (MSD) was evaluated. The rivet driven head deformation range,  $D_{max}/D$ , measured on the test article, was between 1.50 to 1.52 for most of the rivet holes, with an average of 1.516. The pitch spacing was 20 mm in the longitudinal (perpendicular to

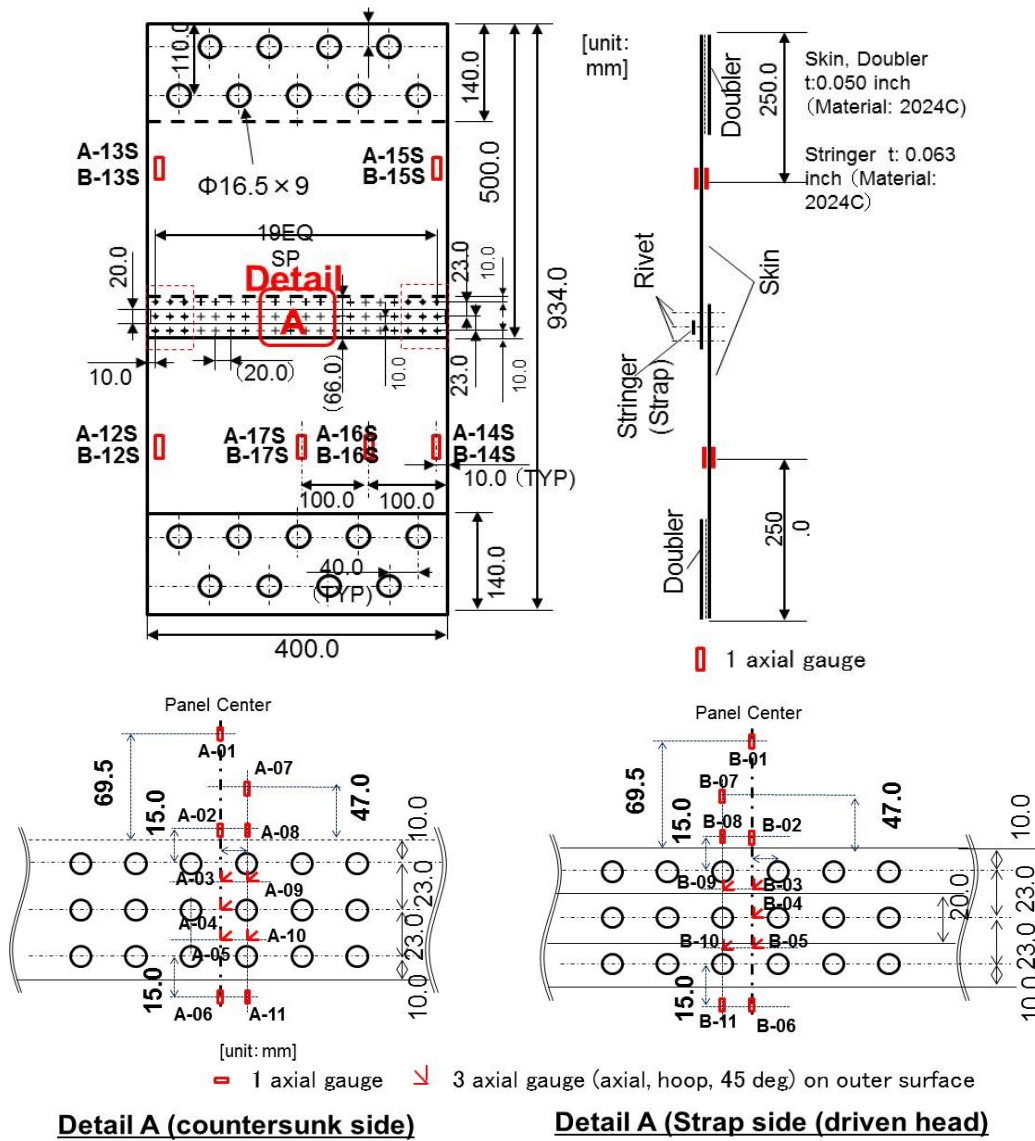


Fig. 1 Specimen configuration and strain gauge locations (dimensions in mm),

loading) direction and 23 mm in the “hoop” (parallel to loading) direction. A total of 24 unidirectional gauges with 5 mm gauge length, KFG-5-120-C1, and 12 rosettes with 1 mm gauge length, KFG-1-120-D17, were used for strain measurements with 2.05-2.11±1% gauge factor. These gauges were categorized in three groups: (i) far field gauges: five pairs at A- and B-12S to 17S, located far away from the overlap section; (ii) near field gauges: six pairs at A- and B-1S, 2S, 6S to 8S, 11S, near the overlap section; and (iii) rosette gauges within the overlap section: seven rosette pairs at A- and B-3R to 5R, 9R, 10R, 18R, and 19R. In this nomenclature, “A” refers to the SGs mounted on the outer surface and “B” refers to the SGs mounted on the inner surface of the joint.

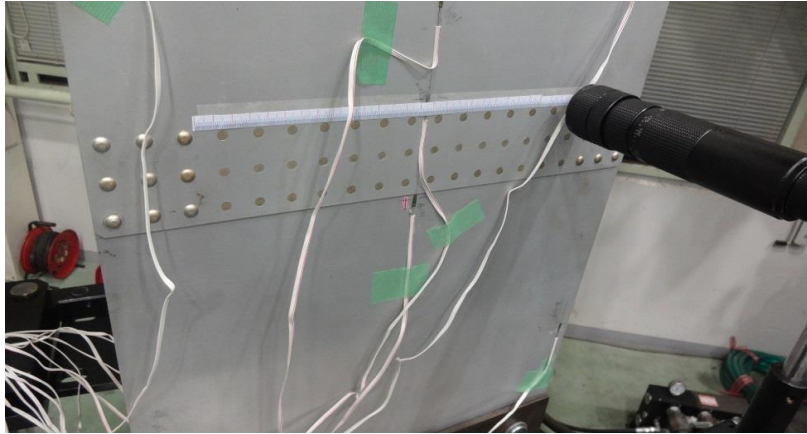


Fig. 2 Fatigue test setup

Static tensile test was conducted first; the tensile load was loaded up from 0 to 42.42 kN (83.5 MPa stress) and then unloaded back to 0 kN for strain data collection. Then tension-tension fatigue test in 10 Hz frequency was carried out with a maximum stress of 65 MPa and a stress ratio of 0.069 for other panel manufactured at same period. During the fatigue test, visual inspection was conducted around each fastener using a 50X magnification charge-coupled device (CCD) camera to detect the locations and lengths of the cracks generated. Fig. 2 shows the setup of the fatigue test. The crack lengths were measured every 10,000 cycles after the first fatigue crack had been detected.

### 3. Prediction of the fatigue life and further crack growth

#### 3.1 Fatigue life prediction

The MSC/Patran FE package (pre- and post-processor) and the MSC/Marc (solver) version 2014r1 were used for the global/local FE model coupling analyses. Static tensile loading analyses were conducted for validation of both the global and local FE models using experimental strain data.

##### 3.1.1 Global/local FE model coupling

###### Global FE model

Due to the symmetric joint configuration, only half of the joint structure was simulated in the global FE model. The generated global FE model is shown in Fig. 3 with 8,713 4-node shell elements and 10,080 nodes, in which fasteners and panel holes were not considered. Shell elements were created at the mid-planes of the panels and strap. The linkages between the fasteners and the panels were modelled using rigid link MPCs (multi-point constraints) which allowed secondary bending to occur under the tensile loading. Only geometric nonlinearity (large displacements) was considered in the global model. A tensile loading step, 0 to 21.21 kN, was applied to the global FE model and MPCs were set for all the right side pins ensuring they had the same tensile displacement.

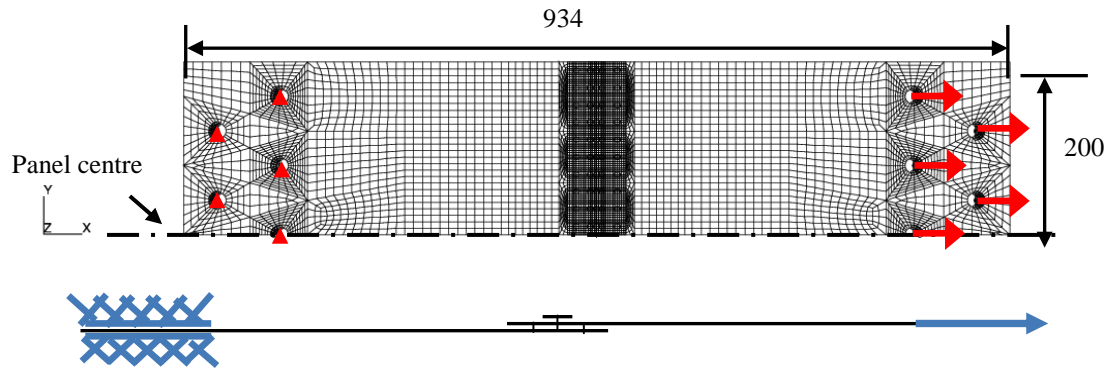


Fig. 3 Global finite element model using shells for the riveted panel joint structure and loaded through pins at the two end sections (dimensions: mm)

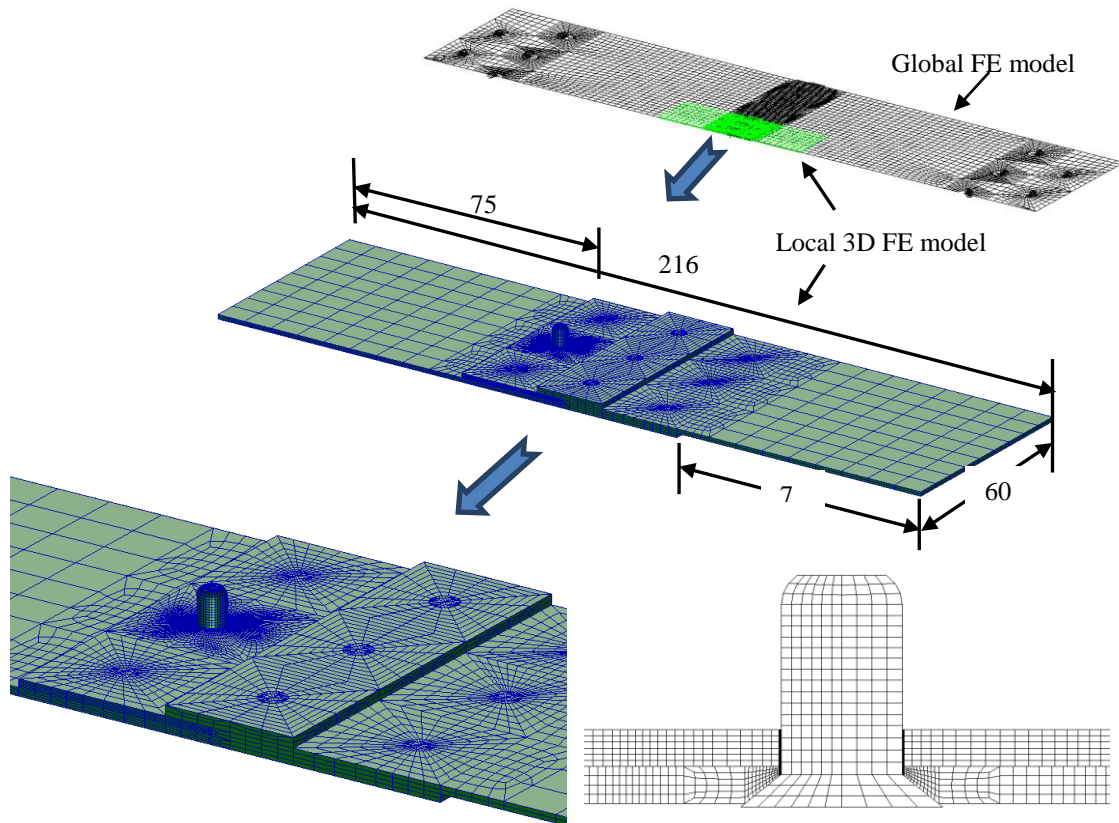


Fig. 4 Schematic presentation for the local 3D model (dimensions: mm)

Local FE model and material parameters

The local model covered nine rivets to avoid edge effects on the stress condition at the top-row rivet, where the riveting process was simulated. For simplicity, eight out of nine rivets were

modelled as “welded” to the panels in the local FE models. The riveting simulation was only performed on the central top-row rivet. The local FE joint model is presented in Fig. 4 with 48,820 8-node reduced-integration contact brick elements and 59,643 nodes. This local joint model had a length of 216 mm in the loading direction (corresponding to the fuselage hoop direction) and a width of 60 mm in the transverse direction (corresponding to the fuselage longitudinal direction). The length of the overlap section was 60 mm. The strap, used to simulate a stringer structure, was assumed welded to the middle row rivets in the local model. The rivet shank diameter,  $D$ , was 3.968 mm. Three local models, with diameters of 4.064, 4.115, and 4.166 mm for the hole protruding part, were created. The corresponding radial clearances between the rivet shank and protruding hole part were 0.048, 0.0735, and 0.099 mm, respectively. The countersunk depth in the outer panel was set to be 0.94 mm, leaving a 0.325 mm thick edge for the hole protruding part.

A fine mesh was applied to the rivet, overlap section and nearby region, while a coarser mesh was used for the panel areas away from the overlap ends. A total of 120 elements were created along the countersunk hole edge perimeter, 6 elements along the inner panel thickness, 4 elements along the protruding edge, transformed to 6 elements in the outer panel hole region. This mesh strategy was determined through a mesh sensitivity study based on the first model (size 1), which had a 0.048 mm rivet-hole clearance. Multiple loading steps from the riveting process to a three-cycle remote loading stage were applied to the local FE mode, in which nonlinearity in material, geometric deformation, and contact boundary condition was considered. It was assumed that the cyclic stress-strain curve (Boller and Seeger 1987) would be stabilized in the third cyclic loading stage. Displacement fields generated at the maximum and minimum remote stress levels were applied to the mid plane nodes around the perimeter of the local 3D FE model to induce the cyclic loading condition. Explanations in the contact pair definition and solution procedure for multiple load cases can be found in author’s previous publications (Li, Shi *et al.* 2007, 2011, 2012),

An isotropic hardening behaviour was assumed for both the rivet and sheet materials. The material parameter of the 2117-T4 Al alloy MS20426AD5-5 rivet (Szolwinski and Farris 2000, Li and Shi 2004, Li, Shi *et al.* 2007, 2011, 2012) is presented in Table 1. The material constants  $C$  and  $m$  were calculated by substituting uni-axial tensile test data into Eq. (1).

$$\sigma_{true} = C(\varepsilon_{true})^m \quad (1)$$

A cyclic stress-strain curve of 2024-T3 in the transverse direction (Boller and Seeger 1987) was used for the skins during the application of the three load cycles. The stress-strain curve (transverse direction) is shown in Fig. 5 with a yield stress of 430 MPa. A Young’s modulus,  $E=70.3$  GPa, and Poisson’s ratio,  $\nu=0.33$ , were used for the sheet material parameters in the elastic deformation stage.

Table 1 Elastic and plastic properties for MS20426ADx-x rivet material.

Parameter of rivet	Value
Young’s modulus $E$	71.7 GPa
Poisson’s ratio $\nu$	0.33
Initial yield stress, $\sigma_y$	172 MPa
Hardening parameters when $0.02 \leq \varepsilon_{true} \leq 0.1$	$C = 544$ MPa and $m = 0.23$
Hardening parameters when $0.1 < \varepsilon_{true} < 1.0$	$C = 551$ MPa and $m = 0.15$

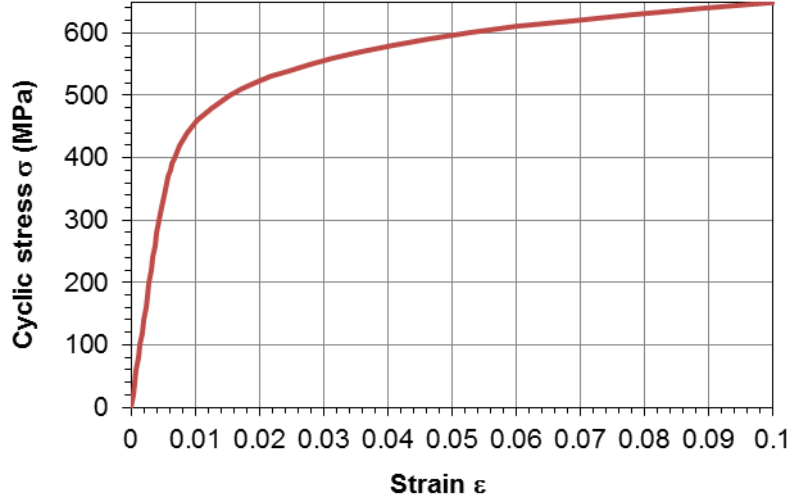


Fig. 5 Stress-strain curve of 2024-T3 Al alloy (transverse direction)

### 3.1.2 Fatigue life assessment

#### Global FE model

The strain-life method was used to estimate the fatigue “initiation” life associated with each combination of hole sizes and rivet deformations. This calculation was performed using the Smith-Watson-Topper (SWT) equation considering mean stress effect

$$\sigma_{\max} \frac{\Delta \varepsilon}{2} = \frac{(\sigma'_f)^2}{E} (2N_f)^{2b} + \sigma'_f \varepsilon'_f \frac{1}{2} (2N_f)^{b+c} \quad (2)$$

where  $\sigma_{\max} \frac{\Delta \varepsilon}{2}$  is calculated at every node of the local 3D FE model in all directions. The maximum calculated value, referred to as the SWT parameter, was used to calculate  $N_f$ , the number of cycles required to meet a predefined “failure” criterion. The SWT equation was derived using the Basquin and Manson-Coffin equations by Smith, Watson *et al.* (1970) for covering the elastic and plastic strain amplitude effects. The Basquin and Manson-Coffin equations are shown in Eqs. (3) and (4) respectively

$$\left( \frac{\Delta \varepsilon}{2} \right)_e = \frac{\sigma'_f}{E} (2N_f)^b \quad (3)$$

$$\left( \frac{\Delta \varepsilon}{2} \right)_p = \varepsilon'_f (2N_f)^c \quad (4)$$

where:  $\sigma'_f$  = the tensile fatigue strength coefficient;  
 $\varepsilon'_f$  = the tensile fatigue ductility coefficient;  
 $c$  = the fatigue ductility exponent;  
 $b$  = the fatigue strength exponent;

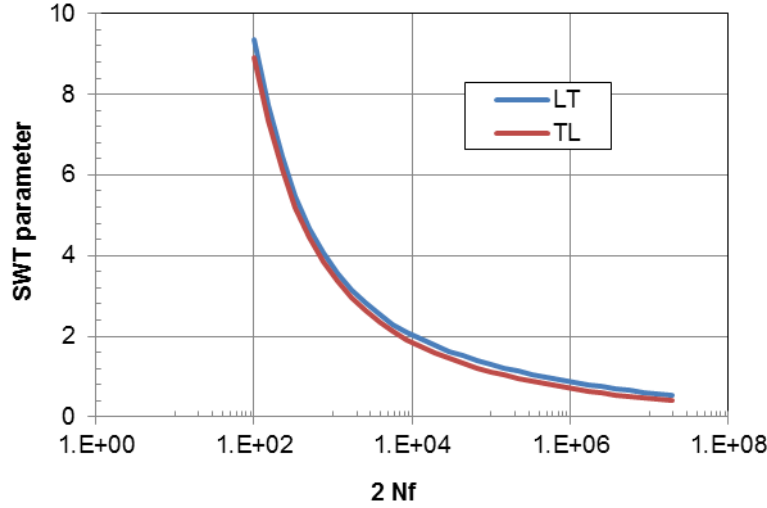


Fig. 6 SWT parameter (MPa) - life relationship

$N_f$  = the number of cycles to get, in this case, a 5% decrease in the tension load of the cylinder coupon (transverse direction in the coupon fatigue test), This can be back-calculated to be approximately equivalent to a 0.5 mm deep crack;

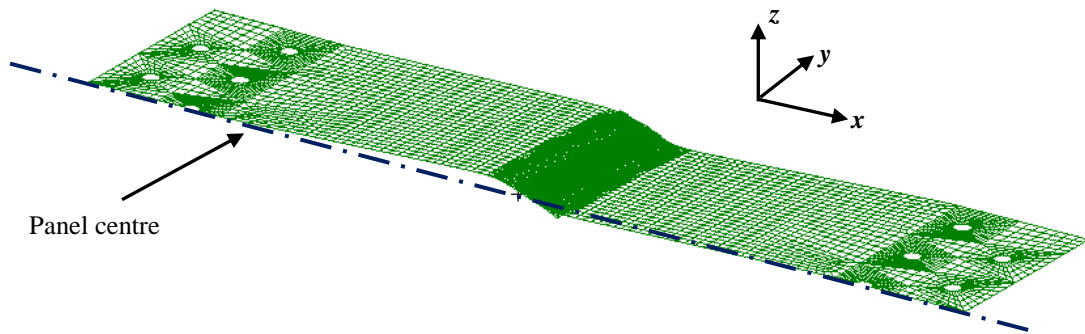
$E$  = the Young's modulus;

$\Delta\varepsilon = \varepsilon_{\max} - \varepsilon_{\min}$  the strain range.

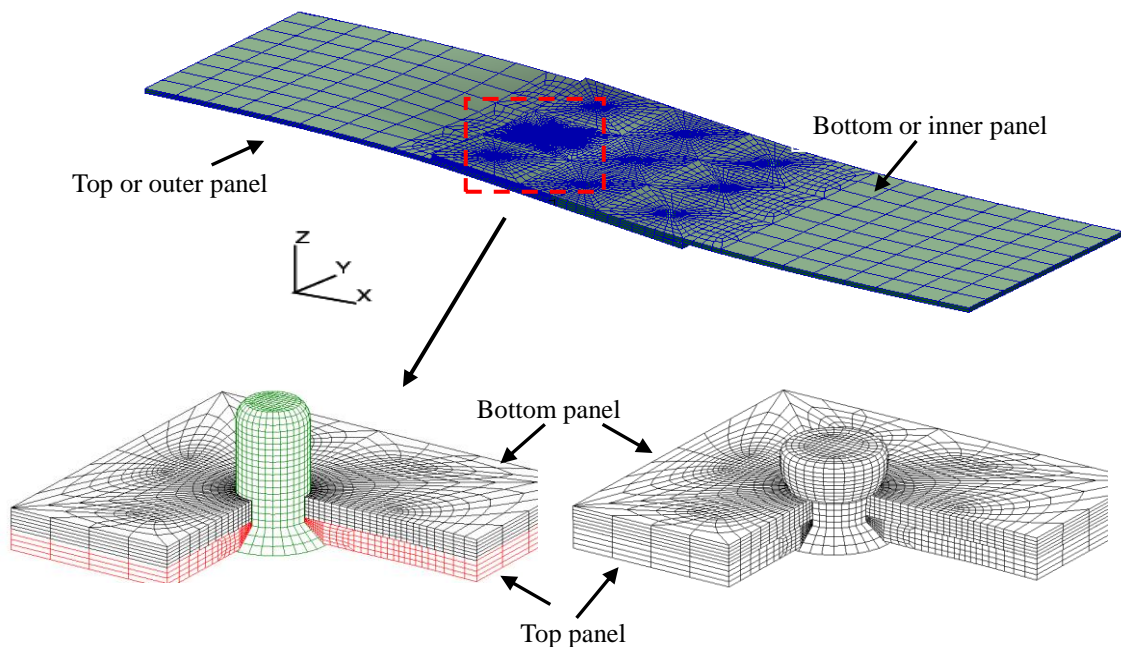
For the 2024-T aluminium alloy sheets, the transverse-direction (TL) strain-life constants were taken from (Boller and Seeger 1987) as:  $\sigma'_f = 835$  MPa,  $\varepsilon'_f = 0.174$ ,  $c = -0.644$ ,  $b = -0.096$ , and  $E = 70.28$  GPa. The relation between the calculated SWT parameter and the "initiation" life is presented in Fig. 6.

### 3.2 Crack growth analysis

Fatigue crack growth from a 0.5 mm crack to the first link-up of two adjacent cracks between two holes was evaluated using the NRC in-house tool, CanGROW, which includes capabilities to perform Monte-Carlo simulations for MSD problems (Bombardier, Liao *et al.* 2010). Correction curves on the part-through crack in a countersunk hole, expressed as functions of crack length, were developed to consider the effects of the riveting induced residual stresses, obtained from the local FE model, and the countersunk geometry. These correction curves were calculated using AFGROW 5.2, which includes a countersunk geometry stress intensity factor solution [20]. Using the AFGROW COM interface, the applied remote load (spectrum) was automatically adjusted, based on the crack tip position, to consider the stress fields under the maximum and minimum cyclic loads, including the post-riveting residual stresses. This strategy was used because the residual stress option was not available for the countersunk geometry in that version of AFGROW. The stress intensity factor curves obtained from AFGROW were then converted to correction curves applicable to MSD cracks located at straight holes in a CanGROW model, which could then be used to estimate the life to the first link-up of the two adjacent cracks (Bombardier, Liao *et al.* 2010, Li, Renaud *et al.* 2014),



(a) Enlarged secondary bending in the global FE joint model in tension



(b) Joint secondary bending (enlarged) and rivet head original and deformed shape predicted by the local FE model

Fig. 7 Joint secondary bending predicted by both global and local FE models. The riveting process was conducted in the local FE model prior to the fatigue loading analysis

## 4. Results and discussion

### 4.1 Joint deformation and strain comparison

Due to the tensile load path eccentricity, secondary bending occurred in the single-lap joint under tension. Fig. 7 shows this deformation feature in both global and local FE models. Rivet driven head deformation was obtained from the local FE model through the riveting process

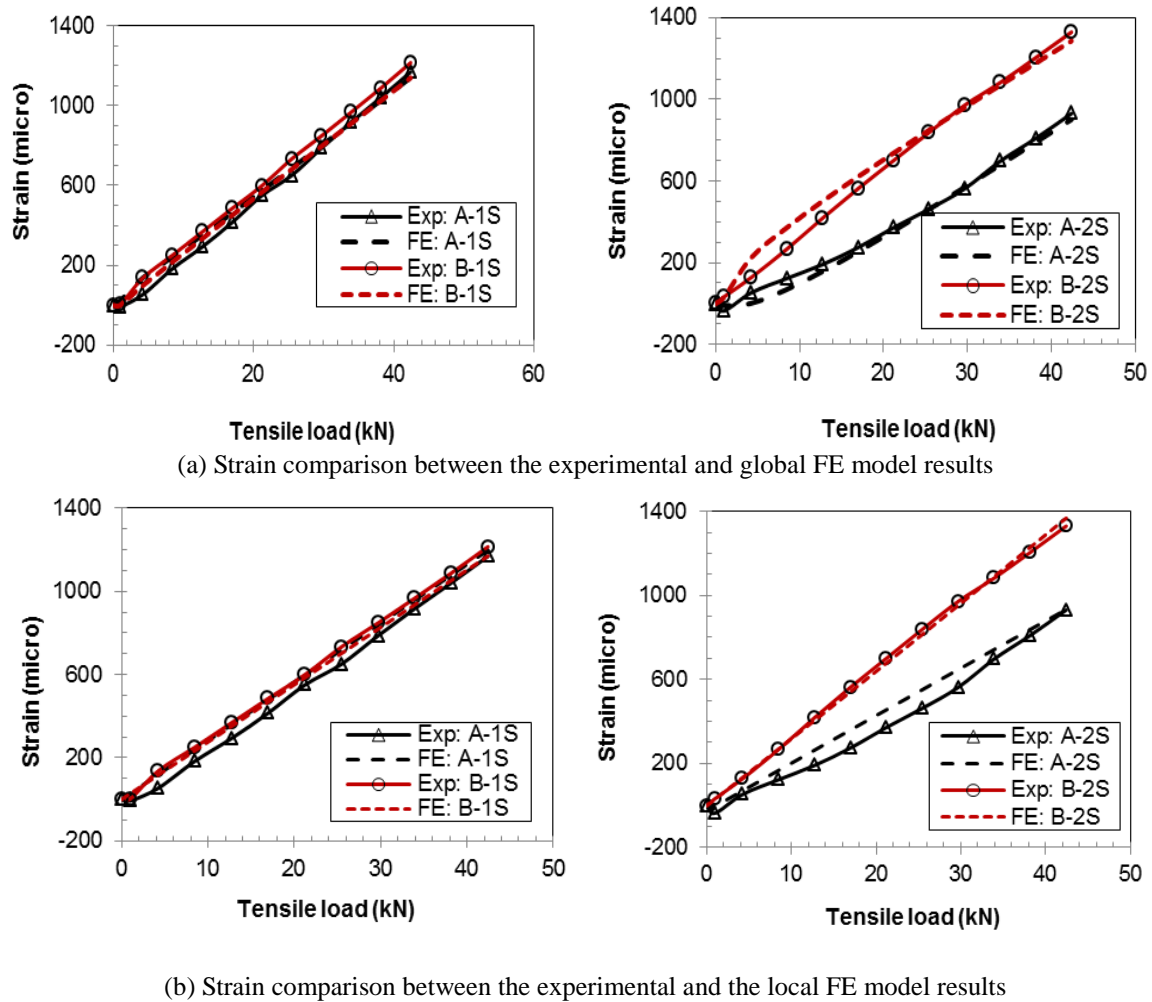


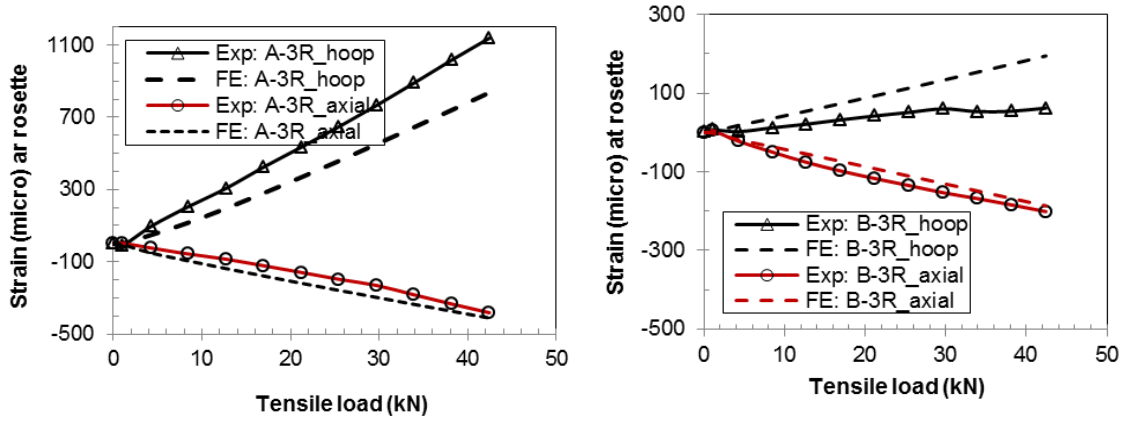
Fig. 8 Strain comparison between the experimental data and the global (a) and local (b) FE models in the field near the overlap section

simulation steps and no penetration was observed between the deformable contact pairs. Good agreement in the rivet deformation was obtained between the experimental and FE results. The rivet head deformations obtained from the FE analysis were from 1.501 to 1.527, whereas the provided experimental data were 1.50, 1.51 and 1.52.

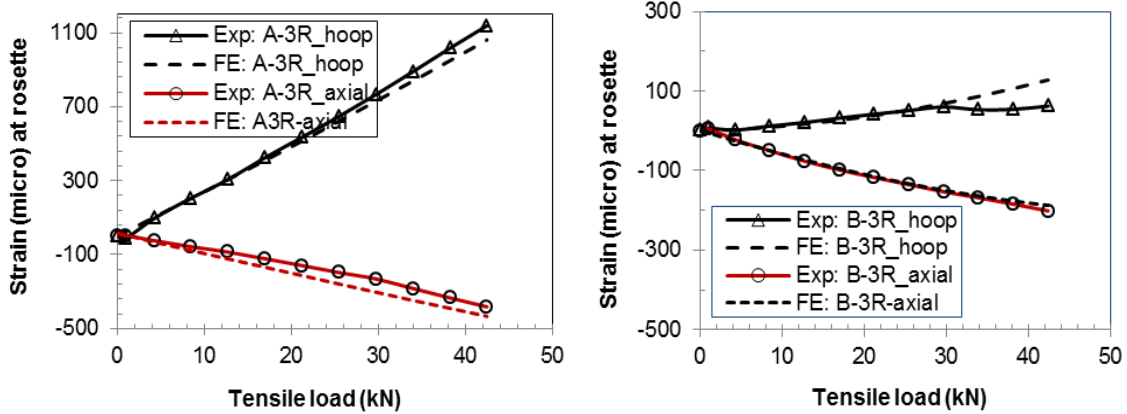
Good correlation was confirmed for most of the SG locations. Strains and stress values in the SG locations obtained from three local models were similar because they were away from the fine meshed area in a radial hoop region equal to  $0.4D$  from the studied hole edge. Strain comparisons at selected key locations were presented only to show the FE model validity.

#### 4.1.1 Strain comparison on the outer panel near the overlap end region

Good agreements between the experimental and FE strains were obtained on the outer panel surface near the overlap end, as shown in Fig. 8 at the SG A-1, B-1 A-2, and B-2 locations. Both



(a) Strain comparison between the experimental and global FE model results



(b) Strain comparison between the experimental and the local FE model results

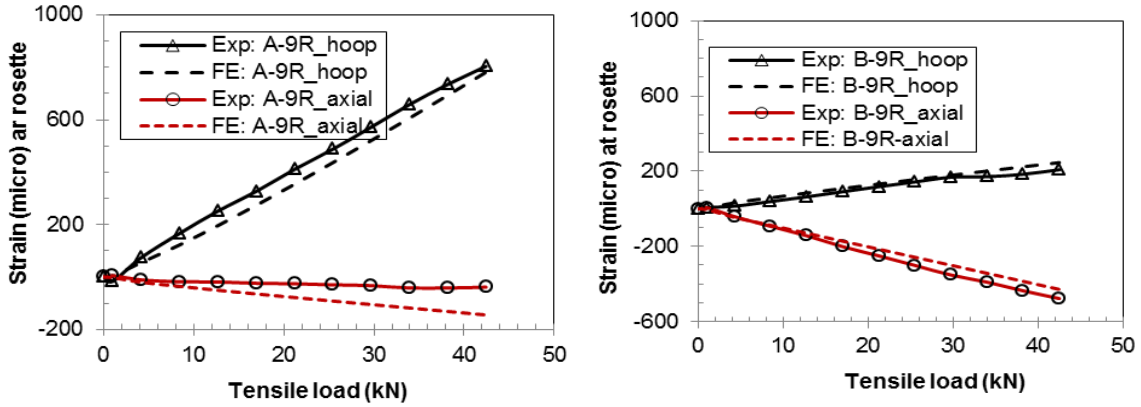
Fig. 9 Strain comparison at the top-row region SG A-3R and B-3R locations between the experimental data and the global (a) and local (b) FE models within the overlap section.

the global and local FE models predicted strains close to the experimental measurements. The little difference between SG A-1 and B-1, located 69.5 mm away from the overlap-end, shows that little bending deformation was present at that location. However, the different strains between the gauges, SG A-2 and B-2, mounted on a 5 mm away from the overlap-end, indicate that secondary bending deformation was present at that location. This comparison clearly shows that the local FE model is valid because it closely predicted the strains for both the bending and non-bending sections

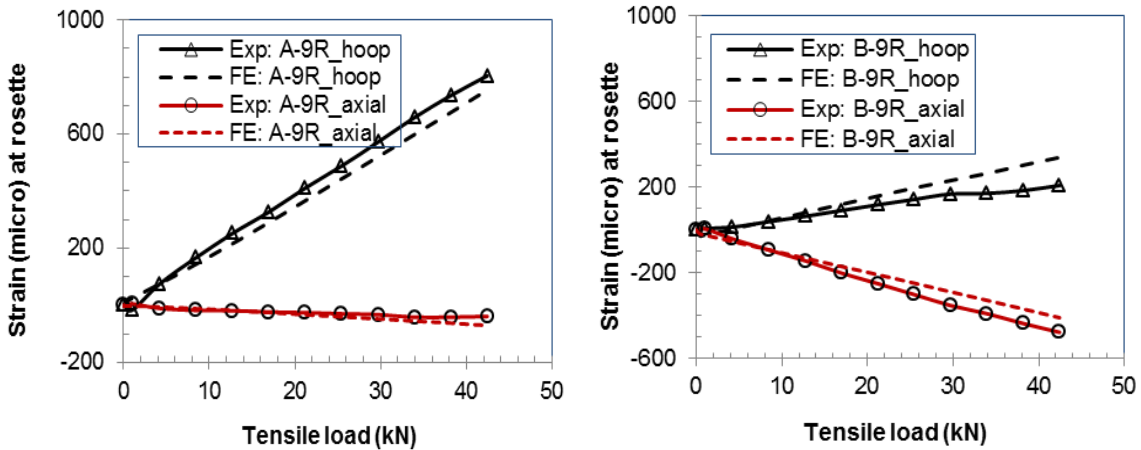
#### 4.1.2 Strain comparison on within the overlap section at the top-row region

Failure was expected to occur in the highly stressed region of the outer panel, within the top fastener row. Therefore, the experimental strains obtained at rosette gauges A-3R, B-3R, A-9R, and B-9S, were compared with the local FE model results to show the model validity.

The rosette gauge A-3R was mounted on the outer surface of the top panel, whereas the gauge B-3R was on the inner surface of the bottom panel. These rosettes were near the top fastener row,



(a) Strain comparison between the experimental and global FE model results



(b) Strain comparison between the experimental and the local FE model results

Fig. 10 Strain comparison at the top-row region SG rosette A-9R and B-9R locations between the experimental data and the global (a) and local (b) FE models within the overlap section

where the top panel was the major load-carrying element. As a result, much higher strains in both hoop and axial direction were present in the top panel than in the bottom panel, which was confirmed by both the experimental and the FE results. It can be seen from Fig. 9(a) that the A-3R gauge reached approximately  $1100 \mu\epsilon$  (microstrain) hoop strain and  $-400 \mu\epsilon$  axial strains, whereas only  $100 \mu\epsilon$  hoop strain and  $-200 \mu\epsilon$  axial strain were measured by B-3R for the 42.42 kN tensile load. In comparison, the global FE model underestimated the A-3R hoop strain by about 27% and overestimated the B-3R hoop strain by about 300%. The axial strains were predicted accurately. The strains obtained in the local FE model were much closer to the experimental values, as shown in Fig. 9(b), For instance, the strain differences were approximately 8% at A-3R hoop direction and 30% at the B-3R hoop direction. The experimental strain in the B-3R hoop direction started decreasing at 30 kN load, whereas the FE results still increased with the applied load. In general, good agreement was obtained between the experimental and FE model results, in which local model improved the prediction accuracy.

Fig. 10 shows that good agreement was obtained between the experimental and FE strain results at the A-9R and B-9R locations. Both the global and local models gave very good strain predictions. Compared with the global model, the local model did not improve the strain agreement at rosette B-9R. However, the local model was considered acceptable based on the fact that this rosette was mounted on the inner surface of the bottom panel, which is not a load-carrying member and has little impact on the joint strength. It is seen that the local model improved the prediction at the A-9R location, located in the top panel at the top-row region, which determines the riveted lap joint strength.

#### 4.1.3 Full-field stress contours and fatigue life prediction

The full-field maximum principal stress contours obtained from the three local models were very similar. The highest stresses were mainly located at the top-row region. Fig. 11 presents the full-field contours on the top panel faying surface obtained from the local size 2 model, with the rivet head deformation of 1.517, under the peak fatigue tensile load condition. The maximum principal stress obtained at the studied countersunk hole, where riveting process was simulated in the local model, is highlighted. It can be seen that the highly stressed regions were very small and mainly located at the hole transverse edge area, perpendicular to the joint tensile direction. This location is in agreement with the joint failure nearly observed in the test.

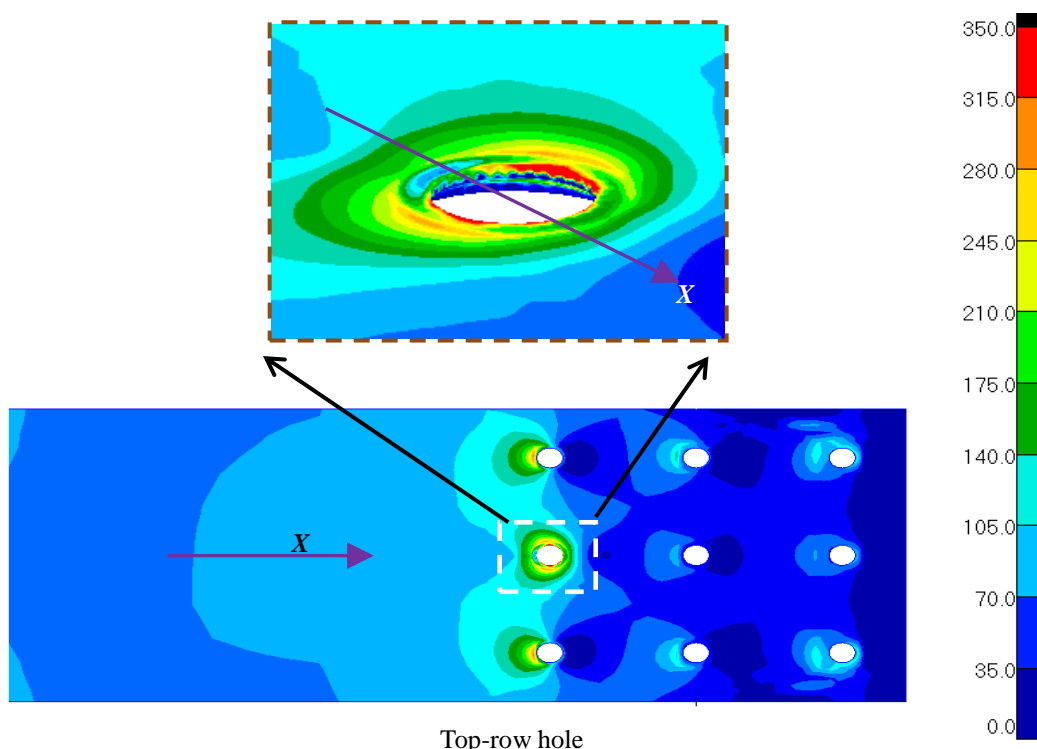
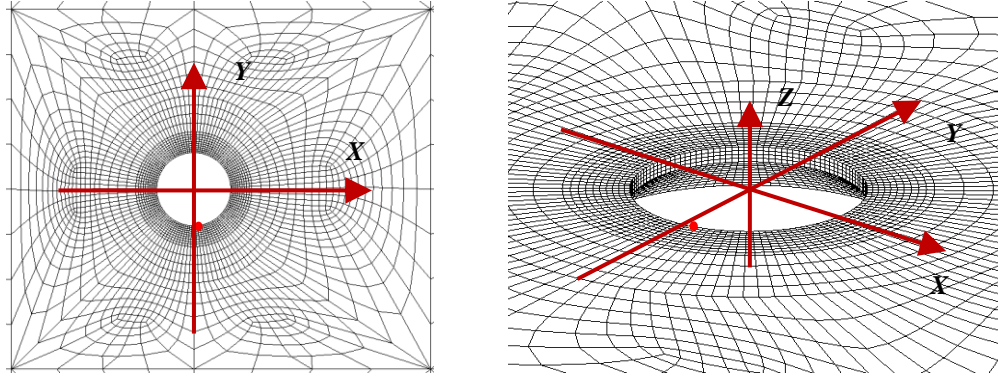
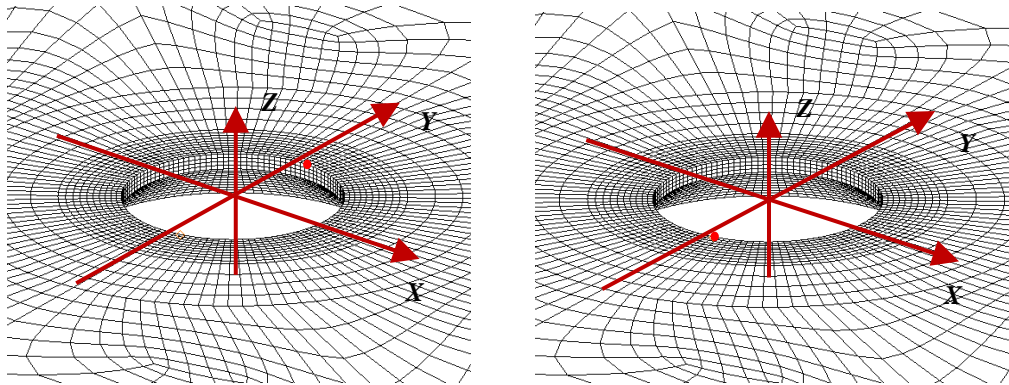


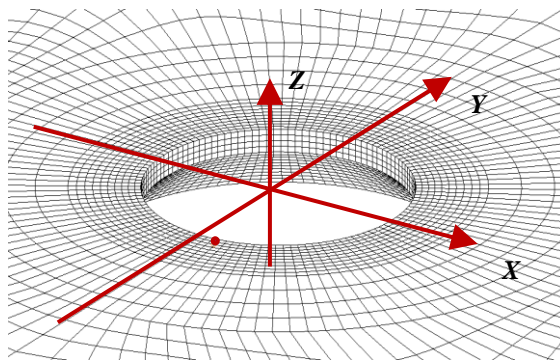
Fig. 11 Full-field contours in the maximum principal stress on the outer panel faying surface and countersunk hole region obtained from the local 3D FE size 2 model with the rivet driven head deformation of 1.517 under the peak cyclic tensile stress of 65 MPa condition in x-direction.



(a) Crack nucleation position (in red) in the size 1 model with the 1.459 rivet head deformation



(b) Crack nucleation position (in red) in the size 2 model with the 1.507, 1.517 (left), and 1.527 (right) rivet head deformations



(c) Crack nucleation position (in red) in the size 3 model with the 1.501, 1.509, and 1.519 rivet head deformations

Fig. 12 The predicted crack nucleation positions (in red) on the top panel faying surface under different driven head deformations of 1.507 and 1.517. The  $x$ -axis is in the global planar remote tensile direction

Table 2 Predicted lives to 0.5 mm cracks.

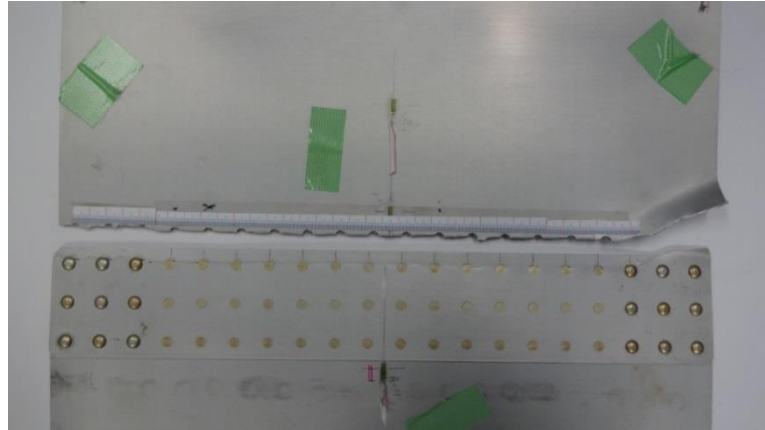
Hole diameter (protruding part)	$D_{\max}/D$ for the countersunk MS20426AD5-5 rivets			65 MPa max stress <b>R=0.069</b>	
	FE	Experimental	Dif. (%)	$\sigma_{\max} (\Delta\epsilon/2)$	$N_f$ (cycles)
Size 1: 4.064 mm	1.459	---	---	0.2608	85.11E+6
Size 2: 4.115 mm	1.507	1.50	0.47	0.5176	2.4337E+6
	1.517	1.51	0.46	0.4851	3.4020E+6
	1.527	1.52	0.46	0.4578	4.5895E+6
Size 3: 4.166 mm	1.501	1.50	0.07	0.5300	2.1526E+6
	1.509	1.51	-0.07	0.5170	2.4471E+6
	1.519	1.52	-0.07	0.5147	2.5031E+6

Fig. 12 shows the crack nucleation sites predicted by the three local FE models through the SWT parameter. These nucleation sites were at very similar positions; they were on the top panel faying surface, at the hole transverse edge area. These predicted crack nucleation sites are consistent with the high stress locations observed in the full-field stress contours shown in Fig. 11.

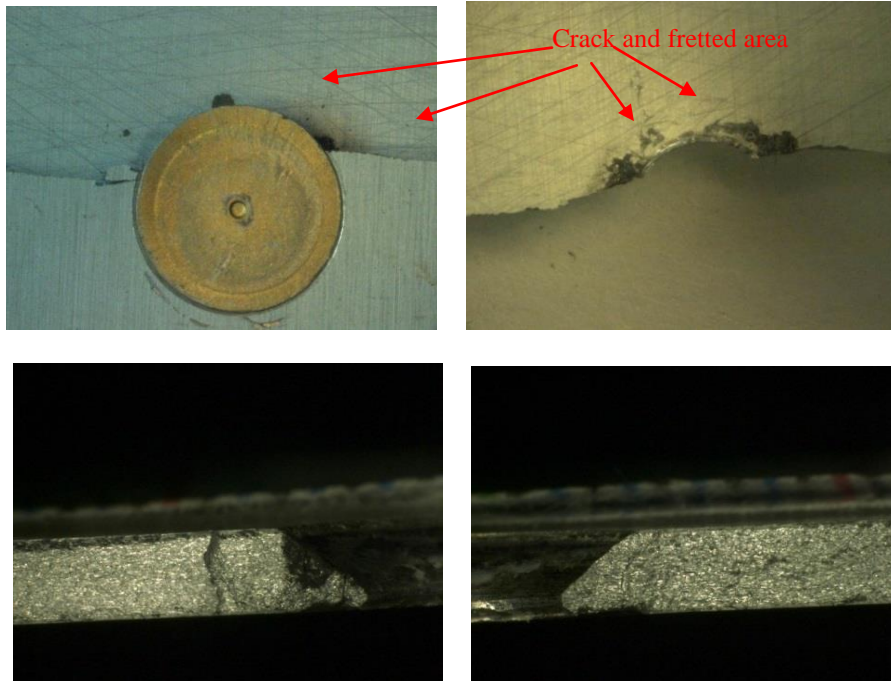
#### 4.2 Predicted fatigue life and test results

Table 2 lists the fatigue lives to a 0.5 mm crack predicted by the SWT equation using the stresses and strains extracted from the three local models.

Rivet driven head deformations of 1.50, 1.51 and 1.52 were referenced to select proper riveting displacement in the local 3D size 2 and 3 models for obtaining the appropriate rivet deformations (Li and Shi 2004, Li, Shi *et al.* 2007, 2011, 2012), The size 1 model, although still within the specification with a radial rivet-hole clearance of 0.048 mm, resulted in lives exceeding 85 million cycles even at the 1.459 rivet deformation. Therefore, further fatigue life assessment in this size 1 model with higher rivet deformations such as 1.50 and above was not conducted. Numerical results showed that the effects of hole size and rivet deformation on the fatigue life were significant. The SWT parameter was found to be very sensitive to the local stress and strain states that are induced by the rivet-hole clearance and rivet head deformation levels in this study. The fatigue lives predicted from the size 2 and 3 models, with radial rivet-hole clearances of 0.074 mm and 0.099 mm, ranged between 2.15 and 4.59 million cycles. The predicted lives obtained from the size 2 and 3 models were slightly higher but relatively close to the JAXA experimental fatigue life of about 1.95 million cycles. The predicted high stress distribution, shown in Figs. 11 and 12, and fatigue life in Table 2 are in relatively good agreement with the failed joint results shown in Fig. 13. The fatigue fracture occurred at the top-row position of the outer panel, and fretted areas were found in the hole edge vicinity on the faying surface and fractured surface. The observed cracks nucleated in the fretted area in the hole edge vicinity area and then propagated along a transverse path. The numbering of the rivet hole starts on the left side of the panel in Fig. 13. Ten through cracks and 19 part-through cracks were identified by fractography. During the fatigue test, the first crack was observed at about 1.95 million cycles at the right side of rivet no. 4, and the second crack was found at about 1.955 million cycles at the left side of rivet no.12. The first link-up of two fatigue cracks was at about 2.11 million cycles between rivet no. 4 and 5 and the structure finally fractured at 2,133,534 cycles.



(a) Fracture occurred at the top-row position of the outer panel



(b) Fretted areas of the outer panel

Fig. 13 Failure information observed from the failed joint under fatigue testing

#### 4.3 Correlation between the crack growth analysis and the test result

A preliminary assessment of the fatigue life to first link-up was carried out using the size 2 hole diameter and the 1.517 driven head deformation. These values were assumed to be, amongst the cases presented in Table 2, the closest to the test nominal rivet diameter and measured deformation. The corresponding analytical life, 3.402 million cycles, was assumed to be the median life to a 0.5 mm crack. Also, a standard deviation of 0.1296 for  $\text{Log}_{10}(\text{life})$ , used in DEF

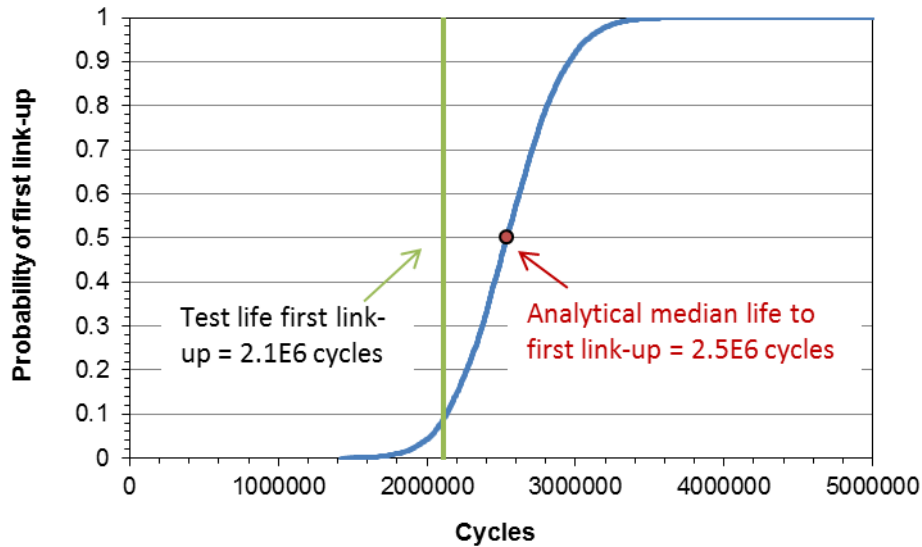


Fig. 14 Stress probability of first link-up within 14 holes

STAN 00-970 (PART 1/5, SECTION 3, LEAFLET 35) recommended for metallic airframe full scale tests, was assumed in order to generate a time to a 0.5 mm crack size (TTCS) distribution. The stresses predicted by the local model were then used in AFGROW to generate a correction curve that included the effect of the riveting residual stresses and countersunk geometry. This correction curve was then used in CanGROW to generate an equivalent initial flaw size (EIFS) distribution by regressing the predicted TTCS distribution to time zero. It should be noted that, EIFS used here is not for life prediction; it is just used in CanGROW to conveniently grow a crack to 0.5 mm and then continue grow the crack to the first linkup. A MSD Monte Carlo simulation of 45,000 trials, each consisting of different random initial cracks sampled from the EIFS distribution and positioned at two adjacent rivet holes, was then performed to estimate the distribution of life to crack link-up between the two holes. When considering the 13 potential link-ups between the 14 adjacent holes, the median of the combined probability of first link-up was calculated to be approximately 2.5 million cycles, as shown in Fig. 14. Good correlation was obtained between first link-up assessment and experimental result in the fatigue life. It should be noted that so far, only one lap joint test was completed and used for comparison. The comparison can be further improved when more results become available.

## 5. Conclusions

A computational methodology was used to predict the fatigue life of a riveted lap joint using a global/local FE model coupling approach and the Smith-Watson-Topper (SWT) equation. The global/local FE modelling was conducted to obtain the stress and strain distributions around the joint, and good correlation was observed between the experimental and FE results. The predicted highly stressed area at the top-row region on the outer panel faying surface and the crack nucleating locations agree with the test observed. The stress and strain conditions, induced by the

riveting process and the remote cyclic loading, were extracted from the local models, and used in the SWT equation to predict fatigue lives to 0.5 mm long cracks. The prediction compared reasonably well with the JAXA experimental fatigue life. Numerical results showed that the effects of the hole size and rivet deformation on the fatigue life were significant.

NRC's in-house tool, CanGROW, was used for a preliminary Monte Carlo simulation for fatigue life to the first link-up between cracks. Good correlation was obtained between the first link-up prediction and tested fatigue life. The calculated distribution was based on an assumed life standard deviation. If more hole measurements became available, a more accurate fatigue life distribution, with a higher degree of confidence, could be developed. This life distribution could then be used for evaluating the WFD behavior, and determine special inspection program.

## Acknowledgments

The work was performed with financial support from NRC and JAXA collaborative projects. A part of NRC's effort was also supported by the Department of National Defence (DND) Canada.

## References

- Anderson, B.L., Hsu, C., Carr, P.J., Lo, J.G., Yu, J. and Duong, C.N. (2004), "Evaluation and verification of advanced methods to assess multiple-site damage of aircraft structures", DOT/FAA/AR-04/42,I, U.S. Department of Transportation, Federal Aviation Administration.
- Boller, C. and Seeger, T. (1987), *Materials Data for Cyclic loading, Part D: Aluminium and Titanium Alloys*. Elsevier Science Publishers, Amsterdam, The Netherlands.
- Bombardier, Y., Liao, M. and Renaud, G. (2010), "A new crack growth analysis tool for the assessment of multiple site fatigue damage", *Proceedings of Aircraft Airworthiness & Sustainment Conference 2010 (AA&S2010)*, Austin, TX, USA.
- Eastaugh, G.F., Straznicky, P.V., Krizan, D., Merati, A.A. and Cook, J. (2000), "Experimental study of the effects of corrosion on the fatigue durability and crack growth characteristics of longitudinal fuselage splices", *Proceedings of the Fourth DoD/FAA/NASA Aging Aircraft Conference*, St. Louis, USA.
- Grandt, Jr. A.F.G., Farris, T.N. and Hillberry, B.H. (1999), "Analysis of widespread fatigue damage in aerospace structures", Final report for US Air Force of Scientific Research, Grant number F49620-98-1-0293.
- Harter, J.A. (2008), "AFGROW users guide and technical manual, AFGROW for windows XP/VISTA, Version 4.0012.15", AFRL-VA-WP-TR-2008-XXXX, Air Vehicles Directorate, Air Force Research Laboratory, Wright-Patterson AFB, OH.
- Huang, W., Wang, T.J., Garbatov, Y. and Soares, C.G. (2012), "Fatigue reliability assessment of riveted lap joint of aircraft structures", *Int. J Fatigue*, **43**(10), 54-61.
- Li G., Renaud, G. and Liao M. (2014), "Life prediction for a riveted flat panel joint using global/local FE modelling", NRC Report, LTR-SMM-2014-0096, 2014.
- Li, G. and Shi, G. (2004), "Effect of the riveting process on the residual stress in fuselage lap joints", *Can. Aeronaut. Space J.*, **50**(2), 91-105.
- Li, G., Shi, G. and Bellinger, N.C. (2007), "Residual stress/strain in three-row countersunk riveted lap joints", *J. Aircraft*, **44**(4), 1275-1285.
- Li, G., Shi, G. and Bellinger, N.C. (2011), "Stress condition in triple-row riveted lap joints under the influence of specific factors", *J. Aircraft*, **48**(2), 527-539.
- Li, G., Shi, G. and Bellinger, N.C. (2012), Chapter 6: "Assessing the riveting process and the quality of riveted joints in aerospace and other applications", *Welding and joining of aerospace materials*, Ed. M.C.

- Chaturvedi, Woodhead Publishing Limited, Cambridge, UK.
- Liao, M., Bombardier, Y., Renaud, G. and Bellinger, N.C. (2010), “Advanced damage tolerance and risk assessment methodologies and tools for aircraft structures containing multiple-site and multiple-element fatigue damage”, *J. Aerospace Eng.*, **226**(11), 2010.
- Liao, M., Shi, G. and Xiong, Y. (2001), “Prediction of fatigue life distribution of fuselage splices”, *Int. J. Fatigue*, **23**, S177-185.
- MSC/Patran, Global/local model using FEM Fields, PATRAN 302 Exercise workbook-release 8.0, 19-122. [http://web.mscsoftware.com/support/online\\_ex/previous\\_Patran/Pat302/Exercise\\_19\\_FEM\\_Global\\_Local.pdf](http://web.mscsoftware.com/support/online_ex/previous_Patran/Pat302/Exercise_19_FEM_Global_Local.pdf), cited on Dec. 2014.
- Müller, R.P.G. (1995), “An experimental and analytical investigation on the fatigue Behaviour of fuselage riveted lap joints: The significance of the rivet squeeze force and a comparison of 2024-T3 and glare 3”, Ph.D. Dissertation, Delft University of Technology.
- Newman, Jr. J.C. and Ramakrishnan, R. (2016), “Fatigue and crack-growth analyses of riveted lap-joints in a retired aircraft”, *Int. J Fatigue*, **82**, 342-349.
- Silva, L.F.M., Goncalves, J.P.M., Oliverira, F.M.F. and de Castro, P.M.S.T. (2000), “Multiple-site damage in riveted lap-joints: experimental simulation and finite element prediction”, *Int. J. Fatigue*, **22**(4), 319-338.
- Skorupa, A. and Skorupa, M. (2012), *Riveted Lap Joints in Aircraft Fuselage: Design, Analysis and Properties*, Springer.
- Smith, K.N., Watson, P. and Topper, T.H. (1970), “A stress-strain function for the fatigue of metals”, *J. Mater.*, **5**, 767-778.
- Szolwinski, M.P. and Farris, T.N. (2000), “Linking riveting process parameters to the fatigue performance of riveted aircraft structures”, *J. Aircraft.*, **37**(1), 130-137.
- Trego, A. and Cope, D. (2001), “Evaluation of damage tolerance analysis tools for lap joints”, *AIAA J.*, **39**(12), 2250-2254.